UNIVERSITY
OF TRENTO - Italy
Department of Physics

NANOSCIENCE LABORATORY

HIGHLIGHTS 2017

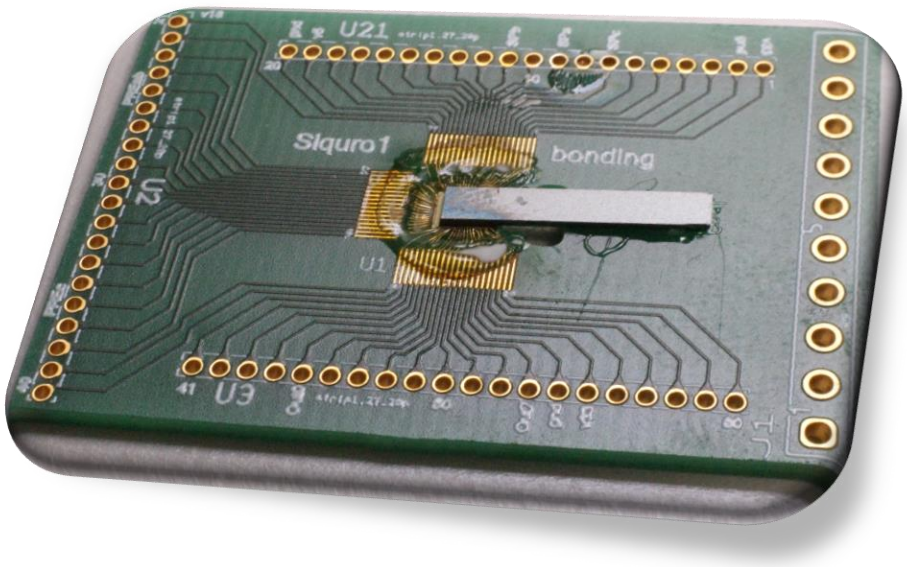

Image on the front cover:
A Quantum Random Number Generator chip: the entropy source is bonded to the detector chip (fabrication by FBK-CMM within the SIQURO project).
Photo by S. Signorini e C. Castellan

NANOSCIENCE LABORATORY

MEMBERS (2017)

Faculty staff

Lorenzo Pavesi (full professor, head)
Marina Scarpa (full professor)
Zeno Gaburro (associate professor)
Paolo Bettotti (assistant professor)
Fernando Ramiro Manzano (researcher, left January 2017)

Technical staff

Enrico Moser
Giorgio Fontana (EP7 level)

Administrative staff

Tatsiana Egorova

Post-doctoral fellows

Mattia Mancinelli (left April 2017)
Massimo Borghi
Pierre Guilleme

Doctoral students

Stefano Tondini (PhD in March 2017)
Zahra Bisadi (PhD in July 2017)
Fabio Turri (PhD in July 2017)
Tatevik Chalyan
Alessandro Trenti
Claudio Castellan
Cecilia Ada Maestri
Chiara Piotto
Stefano Signorini
Sara Piccione
Stefano Biasi
Astghik Chalyan (Guest PhD student)
Foroogh Sarbishe Khozeymeh (Guest PhD student)
Chiara Vecchi

Master students

Davide Bazzanella
Alessandro Marchesini
Niccolò Leone
Matteo Pasini
Domiano Lodi
Alessandra Vendrame
Nicola Ferrari

SCIENTIFIC MISSION

Introduction to the Nanoscience Laboratory

The Nanoscience Laboratory (NL) is one of the scientific groups of the Department of Physics, University of Trento. Its main areas of research are integrated quantum photonics, linear and nonlinear silicon photonics and nanobiotechnologies. The mission of NL is to generate new knowledge, to develop understanding and to spin-off applications from physical phenomena associated with photons and nanostructures. In particular, NL works on applying the nanoscience paradigm to silicon or silicon compatible materials to develop micro and nanosystems compatible with the main driving silicon microelectronics technologies. However, silicon is not the only material studied. Other fields of interest concern the use of cellulose to tailor the properties of nanostructure atom-by-atom or the use of perovskites to investigate their new properties. In addition, a particular emphasis is placed on quantum photonics and its applications.

NL research group consists of more than 20 people with different scientific backgrounds. Researchers from physics, bio-chemistry, materials science and electrical engineering are gathered to form a group of interdisciplinary nature. It is worth mentioning that NL collaborates closely with the Center of Materials and Microsystems, Fondazione Bruno Kessler (FBK). This collaboration spans over the last twenty years and covers such topics as fabrication, testing and application of biomaterials and silicon based devices. Both participate in many common projects. The current ones are: project "On silicon chip quantum optics for quantum computing and secure communications – SiQuro" (financed by the Province of Trento (PAT)) and the project "Integrated SYsteM based on PHOtonic Microresonators and Microfluidic Components for rapid detectioN of toxins in milk and diarY products – SYMPHONY" (financed by the European Commission within the 7th framework). A new tight collaboration is ongoing with the Trento units of CNR-INO, specifically dedicated to implement quantum optics in integrated chip.

Moreover, with the support of FBK and CNR, every two years NL organizes a winter school on optoelectronics and photonics. The last edition "9th Optoelectronics and Photonics Winter School: Integrated Quantum Photonics" was held in Folgaria (Italy) from 26 March to 1 April, 2017. Furthermore, the members of NL are often invited to participate in the organizing committees of international conferences or workshops.

The research activities of NL are mainly supported by the local government (PAT), by the European Commission within the research frameworks, by the Italian Ministry of Education, University and Research (MIUR) and by companies. During the period covered by these Highlights, NL has been and is involved in the following projects: Project FIRB NEMATIC "Nanoporous matErials: self asseMbled blAckboard to study sTructure and InteraCtions of DNA, project SiQuro (supported by PAT within the call Grandi Progetti 2012), project PRIN-MIUR NEMO "Nonlinear dynamics of optical frequency combs", some European projects within the 7th Framework: SYMPHONY (FP7-ICT-2013-10) and "Integrated Reconfigurable sIlicon phonic Switch – IRIS" (FP7-ICT-2013-11). In the same period NL was also involved in the scientific collaboration with FTH S.r.L. on the test and validation of an innovative molecular sensor.

Silicon Nanophotonics

Silicon photonics is the technology where photonic devices are produced by standard microelectronic processes using the same paradigm of electronics: integration of a large number of devices to yield a high circuit complexity, which allows for high performances and low costs. Here, the truth is to develop photonic devices that can be easily integrated to improve the single device performance and to allow high volume production.
We are involved in researching new optical scheme for implementing optical network on a chip by using integrated silicon photonics. Thousands of electrical and optical devices are integrated in a single chip to make reconfigurable optical network. We use the concept of whispering gallery modes, which develop in micro-disks or micro-rings, to study new physics (chirality, frequency comb generation, entangled photon generation) or to develop biosensors for toxin detections. The microresonators are coupled directly with narrow mode SOI (Silicon-on-Insulator) waveguides. High quality factor cavities allow studying fundamental quantum optics concept such Bogoliubov excitation in quantum fluid of light. Series of coupled micro-rings are studied to implement novel scheme of neuromorphic computers where the complex dynamic of the nonlinear resonators allows fast and efficient pattern recognition.
To develop silicon photonics, one further add-on is making silicon to do something that it is not able to do in its standard (bulk) form. Low dimensional silicon, where small silicon nanocrystals or nanoclusters (Si-nc) are developed, is one way to compel silicon to act as an active optical material. With Si-nc LEDs we develop chip size, quantum random number generators. Alternatively, we use the strain to tune the non-linear optical properties of silicon waveguides for the development of new MIR sources (parametric generation via second order effects or frequency comb generation). Nonlinear optics is used to generate pairs of entangled photons, which in turn feed quantum interferometers or integrated quantum photonic circuits. Here, a large effort is spent in order to demonstrate in integrated devices the new properties of quantum fluid of light where the nonlinear photon-photon interaction modify the classical properties of light.

Organic/inorganic nanostructures for life applications

This activity concerns the design, fabrication, characterization and surface modification of novel nanostructures with tunable properties which may find utility in biomedicine or environmental remediation. Our work is at the interface between nanoscience and biology since, besides controlling the peculiar properties due to the nanoscale dimensions, we must make our nanostructures suitable for the integration with biological environments, in some cases taking into account the host responses of living systems. We are currently working with semiconductor and metallic nanostructures, namely silicon quantum dots, titanium or titanium coated nanostructures, gold and silver nanoparticles.
Morphology and optical properties of nanostructured porous silicon encourage the use of this material in the fields of drug delivery, imaging, and tissue engineering. We are studying the coating of silicon nanostructures to increase optical stability and decrease toxicity, moreover conjugation to biological molecules and strategies to increase cell uptake and control intracellular localization are among the objective of this research.
Titanium and titanium coated nanostructures which show hydroxyl-rich interfaces, have a rather good affinity for the water environment and can be used to catalyze processes in aqueous solution. In our Lab, we fabricate water soluble titanium nanotubes with high photocatalytic activity and titanium coated hybrid materials (such as hybrids of Ti and graphene) with peculiar photo-thermal properties.
Gold and silver nanoparticles form *hot spots* that contribute significantly to the surface-enhanced Raman scattering (SERS) phenomenon. This phenomenon produces an amplification of the Raman spectrum of the molecules which are absorbed near the gold or silver hot spot. In this way the detection limit of Raman spectroscopy is strongly decreased and selective identification in situ of a low number of the absorbed molecules (the analytes) is possible. In our Lab we are trying to fabricate porous supports where gold and silver nanoparticles are embedded inside the pores, so forming efficient hot spots.

Experimental facilities

The NL facilities allow for detailed experimental studies in nanoscience, photonics and biotechnologies. Since the effective collaboration with FBK most material processing and device productions are performed within their premises. For photonics, we have facilities to cover the light spectrum from the THz to UV ranges with whatever time resolution is needed. Laser sources comprehends: Ti-sapphire fs-ps laser (1 W average over 1000-700 nm, 2 ps or 70 fs pulses, 82 MHz repetition rate) interfaced with a second harmonic generator and pulse picker; Nd-Yag laser interfaced with an optical parametric oscillator which allows scanning the 400-3000 nm wavelength region (pulse 50 mJ, 10 ns, 10 Hz); TOPAS pumped with an amplified Ti:Sa laser which covers the 1-2.6 μm range with 35 fs, 10 kHz, 3 mJ; three tunable CW lasers (850-870 nm, 1200 - 1700 nm and 1500 - 1600nm) fiber pig-tailed; high power fiber-laser at 1550 nm (1-100 MHz, 50 ps); 4W EDFA and 2W semiconductors amplifiers, several pig-tailed diode lasers, ASE source at

1550 nm and a broad band SLD at 800 nm; three high-power true-CW DPSS single-line laser operating at 532, 473 and 355 nm. Detectors comprehend: visible and infrared photo-multipliers and CCDs, a streak camera with ps resolution, 4K cooled bolometers which cover THz region, avalanche photodiodes for vis and IR ranges plus single photon detectors in the visible and IR. Two home-made MIR single photo counters. To perform spectral analysis several set-ups are available: FTIR and dispersive spectrophotometers, a micro-Raman setup, a micro-FTIR and a UV-vis-IR spectrophotometer (shared with other laboratories), UV-Vis and fluorescence spectrophotometer dedicated to biochemical experiments. Seven dedicated apparata for WG characterization equipped with nanopositioning systems and polarization controllers are available, each one specified on a given functions: visible, quantum, passive infrared, nonlinear infrared, nonlinear MIR, and on-wafer grating. Other apparata are: - visible and infrared photoconductivity set-up; - a solar simulator for cell sizes up to 5 inches; - two nanoprobe stations (AFM and SNOM) - two semiconductor probe stations (4 and 8 inches) and many different electrical characterization set-ups (I-V, Z-Ω, EL-I, etc.). Two VIS to NIR optical spectrum analyzers are available to NL-Lab. A probe station is fiber-bunch interfaced with a spectrometer interfaced with IR and visible liquid nitrogen cooled CCDs. For sample treatment and high sensitivity analytical detection, an electrochemical laboratory equipped with several chemical hots, spinners, galvanostates and voltammeters is available. For optical, electrical and molecular dynamic simulations, the laboratory uses free and commercial software, a dedicated cluster with 16 nodes and work-stations. Two laboratories, one dedicated to chemical synthesis and the second to biological sample preparation, are also available.

SPIE Student Chapter of the University of Trento

SPIE Student Chapter of the University of Trento was established in October 2016. Currently the chapter members are 27. SPIE is the International not-for-profit society for optics and photonics. The majority of chapter members are from our Nanoscience laboratory. The goal of the Chapter is to create a strong community of young researchers from the University of Trento, CNR and Foundation of Bruno Kessler working in various fields concerning photonics and its applications. In this short period, the chapter has organized and participated in numerous public and academic events, such as Day of Photonics, 9th Optoelectronics & Photonics Winter School on Integrated Quantum Photonics, 5th International Symposium on Optics & its applications (OPTICS-2017), PHYSICS2NIGHT within the 103rd Italian National Congress.

On 17th November, 2017 we concluded the chapter first year of activity. In honor of this anniversary, we organized a workshop called "Photonics as a Key Enabling Technology".

As a logical continuation of this productive year, the Chapter has already planned numerous big events for the upcoming year. The most important one will be the 6th International Symposium on Optics and its Applications (OPTICS-2018) on February 17-20, 2018 in Trento, Italy.

2017 publications:

- A. Ghafarinazari, M. Scarpa, G. Zoccatelli, M. Comes Franchini, E. Locatelli and N. Daldosso "Hybrid luminescent porous silicon for efficient drug loading and release", RSC Adv.,7, 6724 (2017)

- A. Lion, N. Laidani, P. Bettotti, C. Piotto, G. Pepponi, M. Barozzi, M. Scarpa "Angle resolved XPS for selective characterization of internal and external surface of porous silicon", Applied Surface Science 406, 144–149 (2017)

- M. Bernard, F. Ramiro Manzano, L. Pavesi, G.Pucker, I. Carusotto and M. Ghulinyan "Complete crossing of Fano resonances in an optical microcavity via nonlinear tuning", Photonics Research, 5 (3), 168-175 (2017)

-Z. Bisadi, G. Fontana, E. Moser, G. Pucker and L. Pavesi "Robust Quantum Random Number Generation With Silicon Nanocrystals Light Source", Journal of Lightwave Technology, 35, 1588 - 1594 (2017)

-M. Mancinelli, A. Trenti, S. Piccione, G.Fontana, J.S. Dam, P. Tidemand-Lichtenbert, C. Pedersen and L. Pavesi "Mid-infrared coincidence measurements on twin photons at room temperature", Nature Communications 8, 15184 (2017)

-C. Piotto, G. Guella, P. Bettotti "Fluorinated surfaces: smart substrates for matrix-free Laser Desorption Ionization", Rapid Communications in Mass Spectrometry, 31 (14), 1228–1230 (2017)

-P.-E. Larrè, S. Biasi, F. Ramiro-Manzano, L. Pavesi, I. Carusotto "Pump-and-probe optical transmission phase shift as a quantitative probe of the Bogoliubov dispersion relation in a nonlinear channel waveguide", Eur. Phys. J. D 71, 146 (2017)

-M. Guarisco, D. Gandolfi, R. Guider, L. Vanzetti, R. Bartali, M. Ghulinyan, M. Cretich, M. Chiari, P. Bettotti, L. Pavesi, C. Pederzolli, L. Pasquardini "A new aptamer immobilization strategy for protein recognition", Sensors and Actuators B 252, 222–231 (2017)

-D. Roilo, C. A. Maestri, M. Scarpa, P. Bettotti, W. Egger, T. Koschine, R. S. Brusa and R. Checchetto "Cellulose Nanofibrils Films: Molecular Diffusion through Elongated Sub-Nano Cavities", J. Phys. Chem. C 121, 15437–15447 (2017)

-M. Borghi, C. Castellan, S. Signorini, A. Trenti and L. Pavesi "Nonlinear silicon photonics", Journal of Optics, 19, 09300 (2017)

-T. Chalyana, G. A.J. Besselinkb, R. G. Heideman and L. Pavesi "Use of Microring Resonators for biospecific interaction analysis", Proc. of SPIE Vol. 10353, 103530Q (2017)

-C. Castellan, A Trenti, M Mancinelli, A Marchesini, M Ghulinyan, G Pucker and L. Pavesi "From SHG to mid-infrared SPDC generation in strained silicon waveguides", Proc. of SPIE Vol. 10358 (2017)

-C. A. Maestri, M. Abrami, S. Hazan, E. Chistè, Y. Golan, J. Rohrer, A. Bernkop-Schnürch, M. Grassi, M. Scarpa & P. Bettotti "Role of sonication pre-treatment and cation valence in the sol-gel transition of nano-cellulose suspensions", Scientific Reports 7, 11129 (2017)

-C. A. Maestri, P. Bettotti and M. Scarpa "Fabrication of Complex-shaped hydrogels by diffusion controlled gelation of nanocellulose crystallites", Mater. Chem. B 5, 8096-8104 (2017)

-S.Signorini, M. Borghi, M. Mancinelli, M. Bernard, M Ghulinyan, G. Pucker, and L. Pavesi "Oblique beams interference for mode selection in multimode silicon waveguides", Journal of Applied Physics, 122, 113106 (2017)

-L. Cenci, C. Piotto, P. Bettotti, A. M. Bossi "Study on molecularly imprinted nanoparticle modified microplates for pseudo-ELISA assays", Talanta 178, 772–779 (2017)

- S. Tondini, C. Castellan, M. Mancinelli, C. Kopp, L. Pavesi "Methods for Low Crosstalk and Wavelength Tunability in Arrayed-Waveguide Grating for On-Silicon Optical Network", Journal of Lightwave Technology, 35(23) 5134 - 5141 (2017)

-R. Bartali, E. Morganti, L. Lorenzelli, V. Micheli, G. Gottardi, M. Scarpa, M. K. Safeen, P. Rajesh, N. Laidani "Oxygen plasma treatments of polydimethylsiloxane surfaces: effect of the atomic oxygen on capillary flow in the microchannels", Micro & Nano Letters, 12(10), 754–757 (2017)

-P. Lecca, F. Bagagiolo and M. Scarpa "Hybrid deterministic/stochastic simulation of complex biochemical systems", Mol. Bio Syst., 13, 2672-2686 (2017)

2017 PhD Thesis:

Stefano Tondini "*Applications of Silicon Photonics: Optical Transport Networks and Quantum Random Number Generators*" (2 March, 2017)

Zahra Bisadi "*All -Silicon-Based Photonic Quantum Random Number Generators*" (24 July, 2017)

Fabio Turri "*Experiments and modelling of vertically coupled microresonators*" (24 July, 2017)

2017 books:

Submicron Porous Materials, editor: Paolo Bettotti, Springer Verlag (2017)

Optical Switching in Next Generation Data Centers, editors: Francesco Testa, Lorenzo Pavesi, Springer Verlag (2017)

1. A robust quantum random number generator based on an integrated structure of the source of entropy and detector (Zahra Bisadi-Giorgio Fontana)

Networking different electronic devices (Internet of Things, IoT) requires the development of low cost, robust and secure communication to protect the links and the data. Therefore, mass manufacturable, integrated, robust and cheap hardware security modules, with a random number generator (RNG) which provides the seed for the digital key generation, are needed.
Silicon technologies are able to provide the required high volume, low cost and small size for IoT applications. Thus, a RNG fully integrated in a small silicon chip might provide an easy implementation of secure protocols in electronic device manufacturing.
The simplest quantum particle which allows the development of quantum random number generators (QRNG) is the photon. A compact QRNG (based on photons) requires the integration of a source and of a detector. We successfully developed a QRNG based on an integrated silicon chip with a single photon avalanche diode (SPAD) and a mini silicon photomultiplier (SiPM) emitter. The structure of the integrated emitter and detector is shown in Fig. 1 . The emitter is an array of 16 pixels, in a double "C" shape. There are two SPAD detectors, one at the left side and the other one at the right side. This will allow the increase of the bit rate by running two QRNG on the same chip. The basic cell of both the emitter and of the detector is realized with a p-on-n junction, in a common n-type epi/substrate. Each cell (i.e. pixel) of the emitter (SiPM) as well as the detector are passively quenched and recharged through integrated resistors. The chips are fabricated in Bruno Kessler Foundation (FBK) in Trento, Italy, using the previously reported "NUV" SiPM technology. [1]

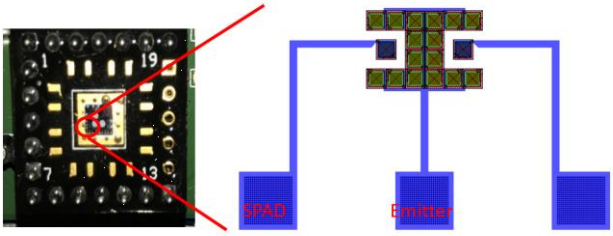

Figure 1. *Image of the packaged chip and layout of the QRNG structure with integrated emitter and two SPAD detectors.*

The emitter and the detector are realized on the same chip, sharing the same cathode bias. The overall bias to the emitter is $V_{emitter} = V_{SPAD} - V_e$, where V_e is the bias applied to one emitter terminal and V_{SPAD} is the bias applied to the SPAD detector. When applying a bias above the breakdown voltage, the emitter SPADs start to be triggered due to thermally generated or background-light-generated carriers, plus all the correlated noise events. During each avalanche some secondary photons are emitted isotropically, a fraction of them reaches the detector, eventually triggering an avalanche in the detector SPAD.
The output signal from the SPAD is amplified, discriminated with an adjustable threshold and sent to a monostable. The digitized signal is then sent to a pulse counter or to an FPGA for random number generation (Fig. 2). The detector has been shielded from ambient light thanks to a top metal layer: only photons from the emitter are detected, making this integrated solution more robust (especially with respect to the ambient light variation).

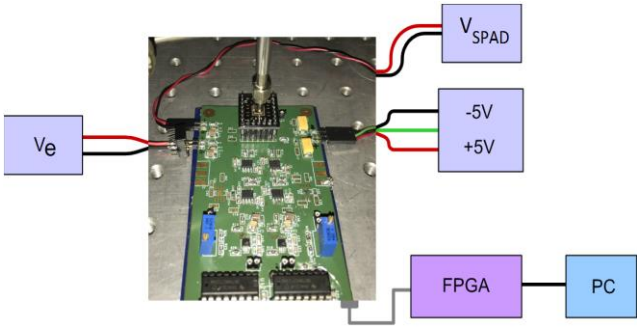

Figure 3. *Schematic of the experimental setup for random numbers generation. The chip board is connected to ±5 V and a bias voltage (VSPAD) is applied to the SPAD. The output signal of the SPAD is transmitted to an FPGA connected to a PC for the generation of random numbers.*

Random symbols are generated using our robust methodology reported in [2]. Considering 1 G symbols:

- ✓ The 2-D visual representation of the generated hexadecimal symbols does not show any particular, periodic patterns.
- ✓ The probability distribution of the symbols is uniform.
- ✓ The analysis of the joint probability mass function shows a departure of ~ 10^{-6} from the theoretical value of 1/16×1/16.
- ✓ Mutual information of the generated random symbols is calculated to be ~ 10^{-7} bits considering.
- ✓ The maximum bias is in the order of ~ 10^{-5} and the min-entropy is computed ~ 3.999 bits per 4-bits.

Substituting each raw random symbol with its corresponding binary "0" and "1" value and applying NIST tests suite, we see that all the statistical tests pass for 1 Gbits. The highest bit-rate is calculated to be ~100 kbps.
The proposed QRNG has still room for improvements both in terms of random bit generation rate and integration level. Therefore, this work represents a first step towards the development of a fully integrated silicon chip which can be used for secure communication in IoT applications.

References

1. NUV silicon photomultipliers with high detection efficiency and reduced delayed correlated-noise. F. Acerbi, A. Ferri, G. Zappala, G. Paternoster, A. Ciotto, A. Gola, N. Zorzi, and C. Piemonte. 2015, IEEE transactions on Nuclear Science, 62, 1318-1325 (2015).
4. Robust quantum random number generation with silicon nanocrystals light source. Z. Bisadi, G. Fontana, E. Moser, G. Pucker, and L. Pavesi, Journal of Lightwave Technology, 35, 1588-1594 (2017).

2. Photonic implementation of Artificial Neural Networks (Davide Bazzanella, Paolo Bettotti)

Artificial Neural Networks (ANN) have formal similarity with biological neural connections. This renders them of interest also as a platform to study and to better understand how human brain works. Moreover, their rich dynamics allow building computational devices which are able to perform complex operations and are highly parallel in doing so. These compare directly with the highly serial and simpler von Neumann architecture of common computers. Apart from the performances, ANN are interesting also because they do not need to be programmed for specific tasks but they need only a training period before being operational.
ANNs are classified into broad categories depending on the topology of the network and of their connections. Feedforward ANN (FFNN) is the first type of ANN developed: its nodes are disposed in layers which elaborates information and pass it on to the next layer. This kind is still the most used, because of its good balance between positive results and simulation complexity, given by its straightforward structure. However, network of this kind are often trained with the Deep Learning (DL) approach, which is particularly costly in time. ANN showing the richest internal dynamics are the recurrent ANN (RNN), where nodes are highly interconnected and show back-propagating feedback among neurons. These ANN are much more difficult to simulate than FFNNs because of the bidirectional signal propagation and for the same reason are especially complicated to train with the DL approach, compared to FFNNs. Nevertheless, RNNs achieve interesting results with another method, Reservoir Computing (RC), which has the great advantage of a much simplified network training. RC is the most common implementation in photonic integrated circuits (PIC). Its richer dynamics allow for simpler structures, compared to other ANN schemes. On the other hand, the complex network internal dynamics prevent the possibility to describe in detail what is going on during network activity and this fact relegates RC as *little-known-but-fascinating-black-boxes*.
Our aim is to implement a photonic ANN node whose nonlinear transfer function can also be simulated into popular libraries (e.g. PyTorch, Keras, TensorFlow, etc.). By doing this introductory step, we will study the most important characteristics of the singular node structure. This will allow us at a later time to efficiently and accurately model the response of complex PIC ANNs before starting their fabrication, thus minimizing errors in this costly and lengthy process.

3. Nanocellulose: structures and properties (Cecilia Ada Maestri, Marina Scarpa and Paolo Bettotti)

Cellulose is a structural polysaccharide representing the most abundant organic polymer on earth. Recently, there has been huge interest in the isolation of new forms of cellulose, with one dimension in the nanometer range. This new biomaterial, which is usually referred to as nanocellulose, can be readily *modified* by *chemical* processes or physical adsorption, shows mechanical strength, high biocompatibility and undergoes self-organization processes producing compact and transparent films (in the dry state) or soft hydrogels (in the wet state). These characteristics render nanocellulose a versatile and sustainable material for applications in many different fields.
In our lab, we study this material in different forms and environments, focusing on its dynamical properties and paying particular attention to its structure and molecular organization. We obtain cellulose nanocrystals (CNC) (Fig. 3a) starting from cellulose soft pulp or food processing wastes. Using aqueous suspensions of CNC we fabricate transparent films by a casting procedure (fig. 3b).

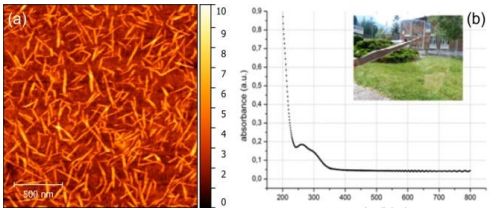

Figure 3. *(a) Atomic Force Microscopy image of cellulose nanofibers. (b) UV-VIS spectrum of a 20 μm thick transparent nanocellulose film (photograph in the inset).*

The interaction of these films with water vapours gives rise to actuation mechanisms, probably due to CNC network relaxation associated to the loosening of the hydrogen bonds. Conversely, these films show excellent gas barrier properties being completely impermeable to small gaseous molecules such as O_2 and CO_2.
On the other side, we observed that CNC in aqueous solution containing small charged molecules, organize themselves forming stable gels with impressive mechanical properties (Fig. 4). This phase transition from liquid to gel has been investigated with different experimental techniques (rheology, nuclear magnetic resonance, infrared spectroscopy and small angle X-ray scattering) and the hydrogel structure has been characterized in terms of mesh size and water exchange dynamics.

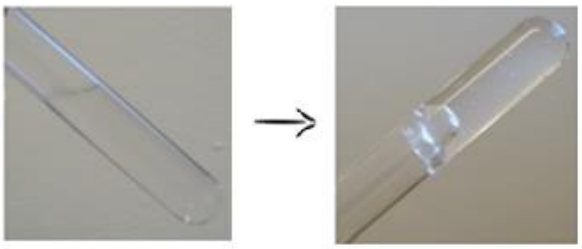

Figure 4. *Sol-gel transition from an aqueous nanocellulose solution to a transparent self-standing nanocellulose hydrogel.*

Ionotropic gelation processes allow to obtain hydrogel objects (Fig. 5), the size and shape of which can be designed by controlling the amount of CNC and gelling agent together with the dynamics of their interaction.

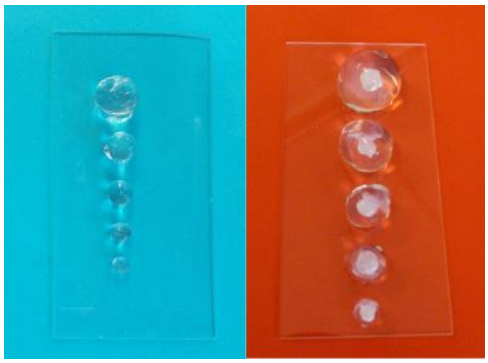

Figure 5. *Beads and capsules obtained by ionotropic gelation using Ca2+ as gelling agent.*

4. Hydrophobic drugs delivery with porous silicon (Chiara Piotto, Marina Scarpa, Paolo Bettotti)

Nowadays several pharmaceutical compounds are administered either orally or intravenously, but since the majority of the drugs are poorly water soluble or, even worst, are non-polar molecules, they suffer from low bioavailability. That's one of the reason why the Drug Delivery Systems (DDS) have been introduced: they are micro- and nano-carriers made of biocompatible and biodegradable materials, that are designed to transport and deliver pharmaceutical compounds to safely achieve a therapeutic effect.

The focus of our work is the study of the interactions of non-polar molecules with nanostructured porous carriers. The molecule that we have chosen as a model is beta-carotene (BC), since it is non-polar and insoluble in water. As porous carrier we work with porous silicon (Psi), that can be fabricated exploiting an electrochemical corrosion process: changing the etching parameters one can obtain different Psi morphologies. Furthermore Psi surface chemistry can be easy tuned to obtain either hydrophilic or hydrophobic Psi samples.

First of all we have studied the BC release from Psi samples with different morphologies. We have loaded Psi using the *impregnation method,* that consists in depositing a drop of BC solution on Psi samples; thanks to capillary force the solution enters the pores; the solvent evaporates and the drug remains inside the porous carrier. After the loading, the samples are immersed in a solvent (ethanol) and the BC release profile have been obtained monitoring the solution absorption spectrum in time.

The cross sectional SEM images of the Psi samples that we have fabricated and the BC released profiles are reported in Fig. 6.

According to our data, about 70% of the loaded BC is released, independently on the Psi morphology.

Since the pore size is much larger than the Bc dimensions we expected fickian release profiles, but if the data are fitted with a fickian curve, the chi square parameters are not very high and the k-coefficients are different, as reported in table 1.

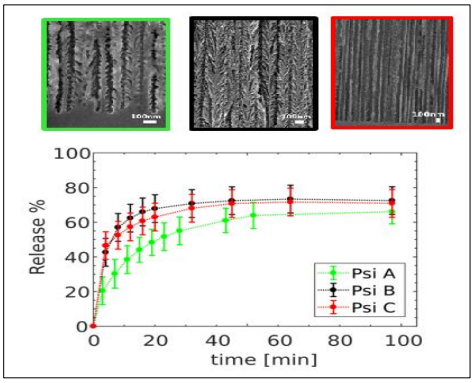

Figure 6. *Cross sectional SEM images of the Psi samples and BC released profiles*

Fickian diffusion: a*(1-exp(-kt))

	Psi A	Psi B	Psi C
k	0.083	0.21	0.22
R-square	0.982	0.992	0.960

Table 1. *Chi square parameters and the k-coefficients obtained fitting the experimental data with a fickian curve*

We found that, even if the BC concentration is lower than its solubility, the BC can nucleate and form aggregates. This can be the reason why the release profiles are non-fickian; in fact if BC aggregates are present, we have to take into account both the molecular diffusion (that shows a fickian profile) but also the aggregate dissolution, that give rise to a non-fickian kinetics.

We exploited also another way to load Psi samples: the *immersion method.* The Psi samples are immersed in a BC solution with known BC concentration (we prepared loading solutions with different concentration of BC) and let that the equilibrium is reached; then the samples are pull out, let drying and transferred in a cuvette, so that BC can diffuse from the samples.

Since we know the BC concentration in the loading solutions and the empty volume of the Psi samples, we can calculate the amount of BC that is inside the pores when equilibrium is reached.

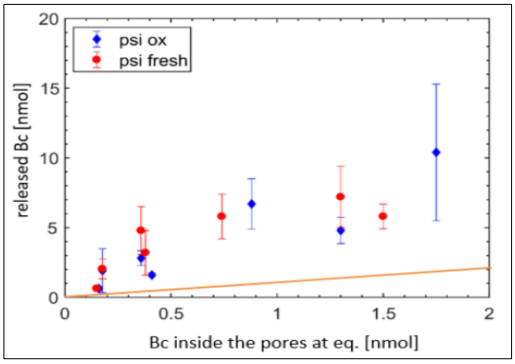

Figure 7. *Nano-moles of BC released from Psi samples as a function of the amount of BC inside the pore at equilibrium*

In Fig. 7 the amount of BC inside the pore at equilibrium vs BC that has been released are reported. Assuming

equilibrium condition is reached, we expected to obtain data on the bisector, instead, the results show that the released Bc is from 5 to 20 times the BC inside the pores at equilibrium. Moreover the standard deviations are very high.
We performed experiments with both hydrophilic and hydrophobic surfaces, but no differences have been observed.
All these considerations led us to think that we do not have only the BC adsorption on the Psi wall but also, BC nucleation and aggregation: that's the reason of the very high irreproducibility.
Both experiments show that, before performing experiments regarding the release kinetics, the study of the loaded molecules physical state is of significant importance.

5. Photonic sensors for mycotoxin detection in milk (Tatevik Chalyan)

The main objective of this work is the development of a sensor for a fast and comprehensive detection of Aflatoxin M1 (AFM1) mycotoxin. Aflatoxins (AFs) are known as poisonous and carcinogenic mycotoxins present in a variety of crops, which can be infected pre-, during and post-harvest.
Looking for a simple and effective method to screen the presence of AFM1 in milk, within the European Project SYMPHONY, we developed an integrated silicon-photonic biosensor based on optical microring resonators (MRR) and asymmetric Mach-Zehnder Interferometers (aMZI). Here, the sensing is performed by measuring the resonance wavelength shift in the MRR transmission or the phase shift of aMZI caused by the binding of the analyte on the functionalized sensor surface. The basic idea behind the aMZI sensor is that the interference at the output of an aMZI is affected by the phase difference between the light, which travels along the two interferometer arms. By opening a window in the cladding layer and exposing one of the two arms to the analyte, the change in the refractive index in the window region is measured as an interference fringe shift in the aMZI output signal. The Mach–Zehnder interferometer is made asymmetric by the addition of a small path length difference between both arms. This difference in path length, results in a wavelength dependence of the output phase.

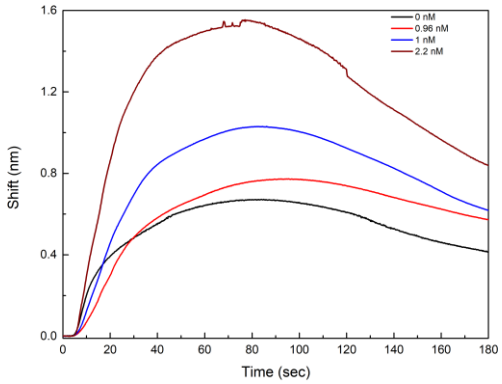

Figure 8. *Sensing measurements of 0.96 nM, 1 nM, 2 nM AFM1 in milk samples and a sample without toxin inside*

From the fringe shift, the phase shift of the light that travels in the exposed arm can be determined. From the resonance wavelength or phase shift, the change of the refractive index is measured, i.e., the sensor can sense the analyte.
With aMZI sensors we demonstrated a high selectivity to AFM1 when Fab'-based functionalization was followed by a casein passivation. For the small concentrations of AFM1, we obtained the linear dependence of the phase shift from the concentration of the toxin.
Finally, the sensor was tested with real milk samples (eluates). Milk is a complex matrix that contains proteins, fat globules, casein micelles, sugars, vitamins and other minor components. In order to increase the toxin detection efficiency in milk and to distinguish the real signal caused by AFM1 binding by Fab', from the non-specific signal, it was needed to first purify and filter the milk. The fully integrated system consisted of three main modules: defatting module, concentrator module and sensor module. After passing through the first two modules, the milk sample flowed over the aMZI sensor surface. A clear difference was observed between registered signals when milk sample was with or without AFM1. For the sensor calibration, the baseline was the phase shift caused by only blank milk sample where AFM1 was not present. We measured AFM1 up to 31 ng/L concentration that was under the EU regulations. Obtained results were compared with ELISA and HPLC.

6. Microring Resonators for real-time study of antibody interaction (Tatevik Chalyan)

In this study (performed during a 3-months internship in LioniX International) we report a system to perform fast antibody interaction analysis using a photonic chip made by an array of six microring resonators (MRRs) based on TriPleX platform. The input light is provided by a Vertical Cavity Surface Emitting Laser (VCSEL) pigtailed to a single mode fiber operating at 850nm wavelength. The output signal is detected by PIN photodetectors placed in an optical signal read-out module (the so-called OSROM). The data were processed by an easy-to-use Fourier Transform algorithm optimized to use most of the available data, reducing the noise. Measured bulk sensitivity (S_b =104 ± 0.04 nm/RIU) and Limit of Detection (LOD = 2 × 10-6 RIU) are very similar for the six MRRs in the same chip, which is a good precondition for using the system for multianalyte detection.

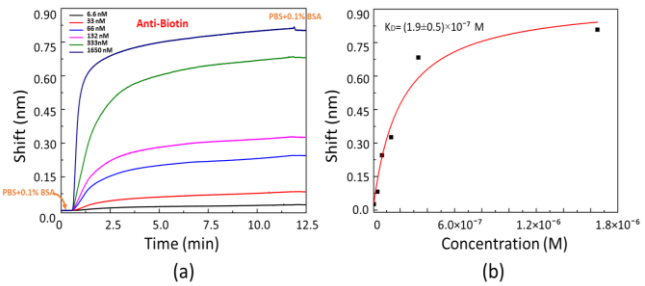

Figure 9. *Sensing measurements of 6.6 nM, 33 nM, 66 nM, 132 nM, 333 nM and 1650 nM anti-biotin-antibody diluted in PBS+0.1% BSA buffer. (a): Sensorgram for anti-biotin different concentrations (b): Langmuir isotherm for the dependence of the sensor response on the concentration of anti-biotin.*

Analyses of anti-biotin interaction with immobilized biotin by using different concentrations of anti-biotin antibody is

performed (see Fig. 9). Dependence of resonance wavelength shift from antibody concentration, as well as association and dissociation rate constants were calculated. For the average dissociation constant (KD) of anti-biotin antibody toward immobilized biotin, a value of 2.3×10-7 M is achieved, that is in the same order of magnitude with published results in literature. Furthermore, the specificity of the interaction was confirmed by using negative control antibodies. In addition, the functional surface of the sensors could be regenerated up to ten times by using 10 mM glycine/HCl pH 1.5.

7. Integrated, scalable and reconfigurable Silicon Photonics based optical network (Stefano Tondini, Astghik Chalyan)

The IRIS project is aimed at demonstrating a transponder aggregator (TPA) switch topology to increase the transport resources utilization in the current optical transport network. The TPA drives 48 optical channels, with 100 GHz spacing in the C-band, 4 different directions and 12 add/drop channels. The IRIS TPA allows colorless (add/drop switching structure is not color specific), directionless (a wavelength can be added/dropped to/from any direction), and contentionless operation (adding/dropping in one direction does not produce contentions for other directions) without external components. It has the highest level of scalability and miniaturization, as it is based on 768 Si double micro-ring resonator (MR) switches, see Fig. 10. The system flexibility, energy efficiency, small footprint and fast re-configurability (microsecond regime) will definitely lead to a paradigm change in the deployment of optical communication in the metro/core segment.

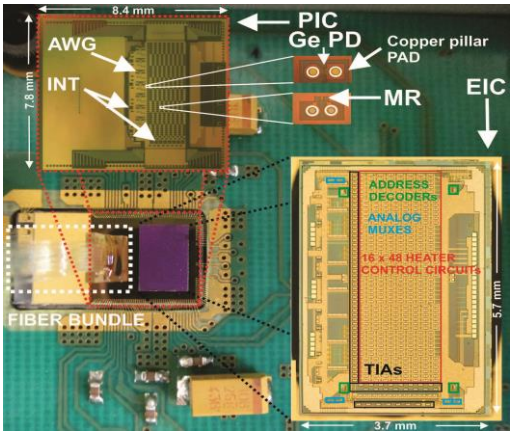

Figure 10. *Electronic-photonic integrated chip wire-bonded to PCB with zoomed photos of photonic IC and electronic IC*

IRIS can be used either as add or drop TPA. To perform the add function, the wavelength channels are added from the local add ports to the output line ports. This can be achieved by simply inverting the direction of the optical flow. The switch nodes are controlled by a 3D-integrated electronic chip, which addresses every single switch through copper pillars from the top (see Fig. 10). The electronic integrated circuit (EIC) allows tuning each photonics component individually: 768 heater control cells are dedicated to the MRs and 56 cells drive the interleavers and de-mux stages. In addition, the EIC reads out the integrated Ge monitoring diodes by means of transimpedance amplifiers (TIAs). MRs, interleavers and de-mux calibration is off-chip performed through a microcontroller. The feedback system implements a stochastic optimization algorithm to align the passband of the photonic components to the waned wavelength. This method allows the automatic initialization of the switch matrix and a microsecond fast reconfiguration of the routing function.

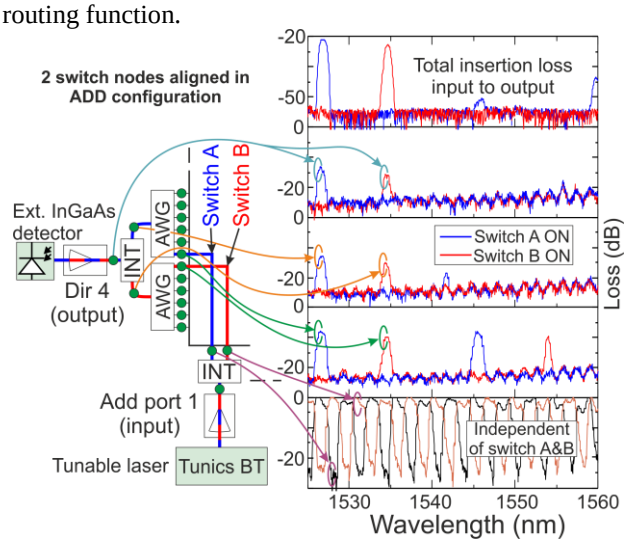

Figure 11. *(left) Schematic of a portion of IRIS working in add configuration. (right) Measured performance of the electronic-photonic integrated chip.*

Fig. 11 shows the response of the switch when one channel is added to a direction for two different scenarios (switch A active or switch B active). It reports the transmission spectra at the different stages within the device. A tunable laser (6dBm) is injected into the input fiber while the transmission at the output is recorded with a InGaAs detector. On the left the signal paths within the chip are shown. The top panel reports the fiber-to-fiber insertion loss, i.e. the transmitted signal at the output with respect to the input signal. We note two high transmission lines due to the selection of the odd or even channel by one of the switches A or B of the switch matrix. Total insertion loss is about -22dB, the channel bandwidth @ -1dB is 60GHz and is 100GHz @ -3dB. The inter channel crosstalk is lower than -35dB. The other panels show the in-the-chip spectra measured by the monitor Ge photodiodes, normalized by the signal from the first photodiode after the input grating. The bottom panel shows the interleaver transmission proving the splitting of the input signal into even and odd wavelengths (almost 0dB device losses on the channels and more than -25dB out of the channels). The other three panels show the spectra on the way through the device: before and after the AWG and after the interleaver. The free spectral range is 19nm and the overall on-chip device loss is about -15dB, which results in total insertion loss of -22dB including the loss of the input/output gratings. In conclusion, the IRIS TPA has a competitive advantage, with respect to existing solutions, of more than an order of magnitude lower cost and overall device volume a factor of 60 smaller (only a few cm^3).

8. Determination of the thermo-optic coefficient and of the nonlinear refractive index of silicon oxynitride waveguides (Alessandro Trenti, Massimo Borghi, Stefano Biasi, Fernando Ramiro Manzano)

Important free-carrier and two photon absorption issues, as well as the band-to-band absorption below ~1 μm of wavelength, limit the use of silicon in several applications. The quest for a transparent, CMOS compatible material, as alternative to silicon, is becoming more and more urgent. For this aim, silicon nitride (Si_3N_4) has been recently investigated, however its use has been hampered by undesired stress that may accumulates at thicknesses over 200 nm, requiring thus specific design and processing solutions. In this framework, silicon oxynitride (SiON) is a very recent appealing material for photonics.

SiON is transparent from the UV to the Mid-infrared (it does not suffer multi-photon absorption losses), it shows minimal insertion losses and it is CMOS compatible. Nonetheless, the silicon oxynitride optical properties have not yet been fully characterized. In particular, very few studies on its linear and nonlinear optical properties have been reported so far.

In our experiment, we studied the thermo-optic coefficient and the nonlinear refractive index n_2 of a relatively high refractive index (n ~ 1.83 at 1.55 μm) SiON. The device under test is an integrated racetrack resonator in the All-Pass filter configuration. A sketch of the top- view of the device is reported in Fig.12.

The racetrack resonator has a cross section of $1.2 \times 0.55\ \mu m^2$ and bending radius of R = 50 μm, while the coupling with the bus waveguide is realized by means of a straight section of length L = 20 μm and a coupling gap of 1.05 μm. The waveguides are single mode for both Transverse Electric (TE) and Transverse Magnetic (TM) polarization at the probe wavelength around 1550 nm.

The thermo-optic coefficient is determined by using a standard, thermally controlled, passive characterization waveguide setup. The device is placed in contact with a Peltier Cell, whose temperature can be tuned in the range 25-75°C with an accuracy ± 1°C. The thermo-optic coefficient has been measured by evaluating the resonance shift Δλ as a function of the temperature variation ΔT. The thermo-optic coefficient results $(1.84 \pm 0.17)\ 10^{-5}\ K^{-1}$, approximately the 74% of the one of Si_3N_4 .

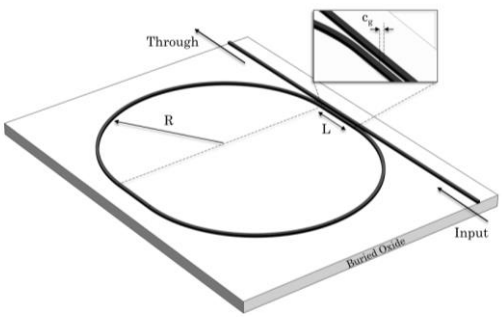

Figure 12. *Top-view of the side-coupled silicon oxynitride racetrack resonator (R = 50 μm and L = 20 μm). The coupling gap is cg = 1.05 μm.*

The nonlinear refractive index is determined from the efficiency of stimulated Four Wave Mixing. An idler beam is combined with the pump laser and injected into the input port of the resonator to stimulate the FWM process. Both the idler and pump wavelengths are tuned on resonance and the generated signal photons, after being optical isolated by more than 100 dB, are detected with a InGaAs photon counter. The value of n_2 results to be $(6 \pm 1) \times 10^{-16}\ cm^2\ W^{-1}$ for the TE polarization, and $(8 \pm 1) \times 10^{-16}\ cm^2\ W^{-1}$ for the TM one. As expected, these values present a clear match due to the isotropic behavior of the SiON amorphous structure.

On average, the nonlinear refractive index of SiON is approximately three times larger than the one of SiO_2 , and the 29.1% of the one of Si_3N_4 .

To conclude, the result reported here envisages that SiON has thermal and nonlinear optical properties which are competing to the other silica or silicon based materials. This shows that SiON is an excellent trade-off platform for the design of nonlinear and quantum optical integrated photonic circuits. in which thermal reconfiguration and nonlinear parameteric processes constitutes fundamental operations.

9. Intermodal Four Wave Mixing in silicon waveguides (Stefano Signorini, Mattia Mancinelli)

Four Wave Mixing (FWM) is a nonlinear optical process widely used in classical and quantum photonics in order to enable several functionalities at the chip scale. Among these functionalities, wavelength conversion and quantum states generation are at the heart of the development of technologies like on-chip gas sensing, mid infrared light detection and generation, quantum information and quantum computing.

The FWM process involves two input pump photons that are converted into signal and idler photons of different frequencies. Usually, the waves involved in FWM excite only the first order waveguide mode. We studied the case of intermodal FWM, which exploits the dispersion of the higher order waveguide modes to control the phase matching condition. In this way, the spectral position of the intermodal phase matching can be easily tuned by engineering the waveguide cross-section, achieving also large detunings from the pump wavelength.

Our work reports the first experimental demonstration of spontaneous and stimulated on-chip IMFWM, using Silicon-On-Insulator channel waveguides. In Fig. 13, we show the spectra of spontaneous IMFWM occurring in waveguides with 2 um and 3.5 um widths and 1.4 cm length. The spectrum of the 3.5-um-wide waveguide exhibits the two discrete bands for the signal and idler wavelengths. The spectrum measured in the 2-um-wide waveguide exhibits only the idler wavelength at 1.2 um, since the signal is generated at about 2.18 um, beyond the detection window of the InGaAs single photon detector used. Our measurements show that we achieved a maximum distance between the signal and idler wavelengths of about 979.6 nm, with the pump wavelength at 1550 nm. We also investigated the tunability of the generated wavelengths as a function of the waveguide width. Several intermodal combinations have been investigated, involving up to the third order waveguide mode.

The high tunability of the discrete phase matched bands, both in terms of spectral position and bandwidth, makes the IMFWM a suitable process for the on-chip development of wavelength conversion devices and heralded single photon sources. Moreover, the large spectral detuning that can be achieved with this process is of great interest for the developing field of mid infrared photonics.

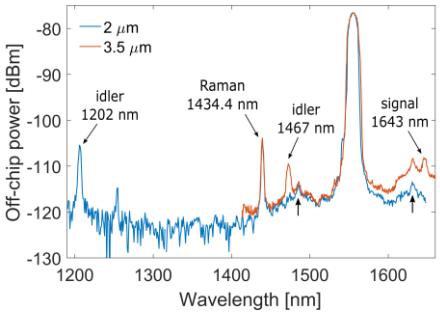

Figure 13. *Spectra of spontaneous IMFWM occurring in waveguides with 2 um (blue) and 3.5 um (red) widths and 1.4 cm length*

10. Four wave mixing control in a photonic molecule made by silicon microrings resonators (Massimo Borghi, Alessandro Trenti)

To overcome the intrinsically weak third order nonlinearity of Silicon, light intensity is coherently enhanced in resonating structures and confined into sub-wavelength photonic wires. The slowing down of light is also an effective tool to increase the nonlinear interaction, since its strength inversally scales with the fourth power of the group velocity. A common scheme to reduce the speed of light uses slow light photonic crystal waveguides. Typically, these structures are treated as a whole, with tens or hundreds of repeating units. Long-range periodicity is deliberately sought to tailor the frequency-wavevector band diagram, in order to increase the group index while keeping the group velocity dispersion reasonably low Dealing with a large number of unit cells makes difficult to understand how to coherently control the strength of some third order nonlinear process, like Four Wave Mixing (FWM), by actively tuning specific sets of internal degrees of freedom. In our work, we experimentally demonstrate that even a simple photonic molecule made by two coupled silicon microring resonators (shown in Fig.14(a)) possess sufficient degrees of freedom for a FWM control which goes beyond the standard enhancement regime observed in slow light waveguides, including also the possibility to suppress the FWM output.
In our experiment, the wavelengths (and the powers) of both the Idler and the Pump laser are kept fixed and resonantly coupled to one of the two resonator of the molecule. Only two parameters are required to set the internal state of the molecule: the inter-resonator phase ϕ and their relative resonance wavelength detuning $\Delta\lambda$. The parameter space $(\phi, \Delta\lambda)$ is spanned by implementing thermo optic phase shifters on the top of the resonators and a Peltier Cell placed in contact with the sample. By direct manipulation of these parameters, coherent collective excitations, analogous to sub-radiance and super-radiance of diatomic systems, can be activated. The increased photon lifetime associated to the sub-radiant state is exploited to enhance the internal field of the constituents of the molecule, thus boosting the FWM signal. On the other hand, we can reconfigure the state to have energy equipartition among the resonators, and consequently suppress FWM by making the two Signal waves to interfere destructively in the bus waveguides.

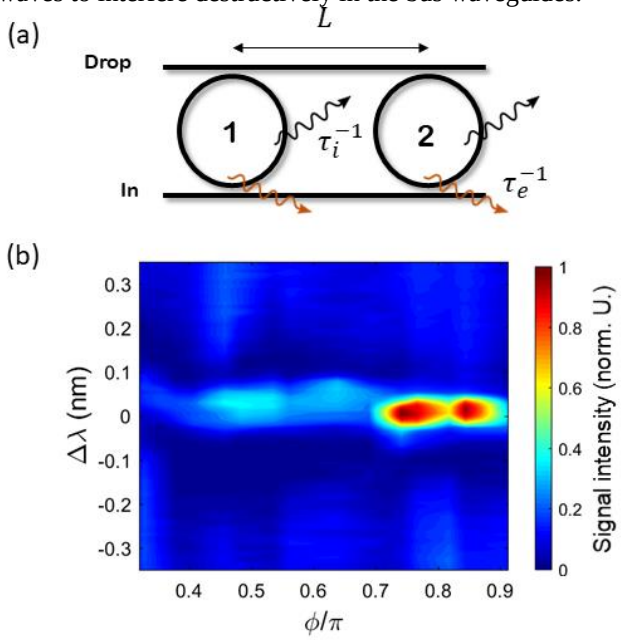

Figure 14. (a) *Sketch of the photonic molecule. It is made by two ring resonators, labelled 1 and 2, separated by a distance* $L = 53.01\ \mu m$ *and indirectly coupled by two bus waveguides. The resonators have a radius of* $6.5\ \mu m$*, intrinsic photon lifetime* $\tau_i = 250\ ps$ *and extrinsic (associated to an energy decay in the waveguide) photon lifetime* $\tau_e = 75\ ps$*. (b) Signal intensity as a function of the wavelength detuning* $\Delta\lambda$ *between the resonator 1 and 2 and the inter resonator phase* ϕ*.*

These different regimes can be identified in Fig.14(b), which shows the intensity of the Signal wave, generated by stimulated FWM, as a function of the inter resonator phase ϕ and their resonance wavelength detuning $\Delta\lambda$. Here, a $7\ dB$ enhancing of the FWM signal is measured with respect to the one generated by a single, isolated resonator. We also show that the same control can be applied to spontaneous FWM. The device is then also appealing for the realization of bright sources of correlated photon pairs. We demonstrated that the performance of the molecule, considered as a whole, is superior with respect to its internal constituents. We could just to mention that through sub-radiance, it is possible to overcome the maximum field enhancement of each isolated resonator, which is unavoidably fixed by the critical coupling condition. This work could constitute an important step toward the realization of a new class of devices which simultaneously act as a source of FWM signal and allow its complete coherent control in a compact and relatively simple way.

11. Phase & transmission response of inter-mode coupling in microresonators (Stefano Biasi, Fernando Ramiro Manzano, Fabio Turri)

Microresonators are one of the most important building blocks of integrated photonics. They represent the key component of light guided circuits for a myriad of applications,

ranging from applied photonics to fundamental quantum electrodynamics. The quality factor (Q) quantifies the light storage capacity and defines the figure-of-merit of a microresonator. High quality factor gives rise to strong light matter interaction and enhances phenomena such as slow light transmission, frequency comb, entangled photon generation. Several efforts in material engineering, device design and fabrication processes have been made in order to improve the maintenance of the light in the microresonator and, correspondingly, increase the Q-factor. The light guided inside the microresonator can be absorbed by the medium or scattered on the sidewall roughness. This roughness inherent to the fabrication process represents the typical limiting source of loss in high or ultra-high Q-factor microresonators.

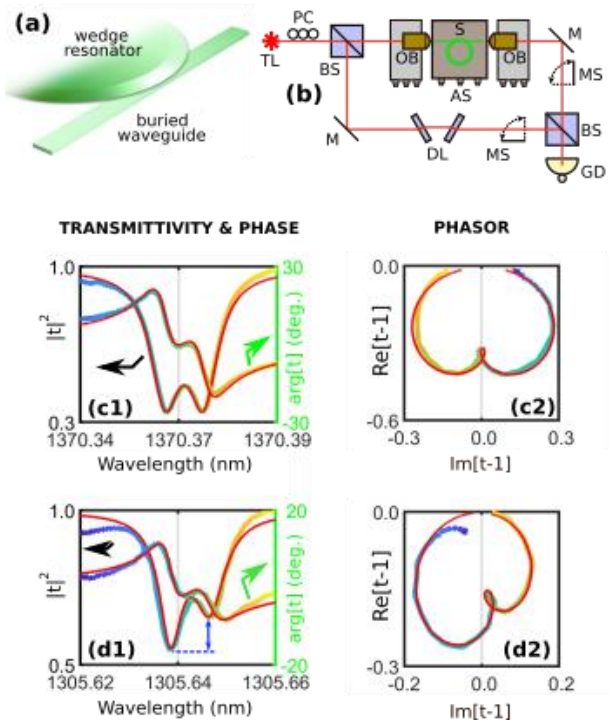

Figure 15. *(a) Sketch of the wedge microdisk resonator. (b) Sketch of the optical Set-up. (c1-d1) Transmission and phase response as a function of the input wavelength. (c2-d2) Parametric phasor plot. The rainbow curves represent the experimental data , while the red lines display the theoretical fits based on the analytical model.*

The surface scattering is typically responsible for a coherent coupling of counter-propagating modes and leads to the formation of new supermodes consisting of linear superpositions of the two clock- and counterclock-wise propagating modes. The roughness modified the typical Lorentzian in the transmission spectra giving rise to a symmetric doublet shape (see Fig.15(c)). However, measurements show an asymmetry between the split resonances in real samples. Experimentally, the asymmetry is observed as different intensities associated to the split peaks (see Fig.15(d)). Theoretical studies have tried to explain this observation by using the temporal coupled mode theory. It has been suggested that the asymmetry might be caused by the interaction of the back-reflections at the bus-waveguide/resonator coupling region, or by the non-linear Kerr-effect.

In our work, we use a novel phase-sensitive set-up based on a free-space Mach-Zehnder interferometer to measure both the transmitted intensity and the phase-shift of the propagating and counter-propagating modes of a silicon nitride wedge-microdisk (see Fig.15 (b)). The interferometer is set in a nearly balanced condition and according to the sketch of Fig.15 (b) the sample is placed into one of its arm. A Germanium detector measures the transmission through either arms or the interference signal as a function of the input wavelength.

The knowledge of both transmission and phase allows using the parametric phasor plots (see Fig.15 (d-c)). This representation puts together the real and imaginay part of the transmission amplitude as a function of the carrier wavelenght. We show that this methods is an analytical tools for characterizing the mode splitting and to estimate the parameters which governs the processes.

We prove that the asymmetry of the transmission response can be well explained in terms of the side-wall anisotropic roughness of the microresonator. In particular, we demonstrate that a non-symmetrical reflection process due to the topology of the roughnesses plays a key role. This assumption does not violate the Lorentz reciprocity principle because the system shows a time-reversal light transmission. However, the reflection remains strongly non-symmetrical under exchange of the incidence direction. This non-reciprocal effect forces a strong unbalanced doublet due to the excitation-direction dependency of the energy distribution between the reflection and absorption. This phenomenon is almost negligible in single-mode high- or ultra-high Q-factor microresonator but it is evident in the case of multimodal microresonators where the reflection and loss channels are increased by the intermodal-mediated coupling. Moreover, we developed a simple model based on coupled-mode theory where the roughness induced both a conservative and a dissipative mode coupling.

12. Power Scaling of Diode Lasers (Sara Piccione)

The study of high power laser work is a new project for the Nanoscience Laboratory, started in November 2016. More in details, the aim of the project is the study and the realization of a high power laser source for Material Processing, with High Power meaning output power of multiple kilowatts.

Nowadays, after communications, material processing with high power laser is the second largest segment of laser applications, concerning global turnovers. Different applications are associated with a defined value of output power and beam quality of the laser beam. Where the beam quality indicates how tightly a beam can be focused. For metal cutting, for example, to have the optimum performance, the beam should have both the highest output power and the highest beam quality. The market of laser for material processing is dominated by three different technologies: The Carbon Dioxide laser technology, the fiber laser technology and the semiconductor laser technology. The CO_2 laser is one the most used laser in industry mainly because guarantees a high output power with a high beam quality. The gain

medium is a mixture of CO_2 and N_2 to improve molecule excitation, placed between an anode and a cathode. The electric discharge causes the excitation of the molecules. The return to the fundamental state causes the emission of a photon. Besides the advantages of the laser, the conversion efficiency is low if compared with other laser technology.
Fiber lasers dominates the high power laser market. The gain medium is an optical fiber doped with rare earth elements, such as erbium, ytterbium or thulium. Since they can have active regions kilometers long, the optical gain coefficient can reach really high values. This translates into the possibility for the fiber to support kilowatt levels of CW output power. The pumping source for the laser is realized by a multitude of semiconductor diode laser, and this is why the fiber laser is also known as brightness converter, since the converts a multi-mode low brightness pump light into a single mode high quality laser beam.
In the past, the semiconductor lasers were used only as a pumping source for fiber and solid-state lasers, but today they have reached the quality necessary to be used as direct sources for material processing applications.
Several reasons led us to choose this particular laser. Among these the highest conversion efficiency, a simpler power and cooling supply, high reliability, small size and a cheaper cost. However, the maximum amount of output power we can get from a single laser cheap is relatively small and the broad bandwidth and low coherence could be detrimental in certain application. Moreover, the beam quality of the laser is low, with respect to the other laser types, and usually different depending on the axis direction.We know that the output power of diode laser linearly depends on the injection current. However, increasing the current does not translate into an increase of the power, because of instabilities of the laser itself.
The solution proposed lies in the combination of several diode lasers. Two different type of combining are possible: coherent and incoherent. The coherent combination of different beams is possible thanks to the constructive interference. To get a high combining efficiency the combined beams must be mutually coherent in both space and time. Therefore, it is necessary the control and the correction of the phase of each of the individual beam, usually done through active algorithms. The incoherent combining is a simpler technique, since the combination is done with beams not having constraints among each other. Three different kind of combining can be distinguished: spatial, polarization and wavelength.The spatial combining is realized by placing the beams next to each other. The power is scaled up, at the expense of the brightness. This combining technique is the one used to realize the pumping sources for other laser type, in which a high brightness is not mandatory. The second combining technique involves the polarization. Two beams with orthogonal polarization could be combined through a polarizing beam splitter. The power increase while the brightness remains equal to the initial one. The limitation is that the combining could happen only with two laser beams.
To efficiently combine several laser beams, it was proposed a novel technique, in which the combining is performed with beams with different wavelength, with the use of a diffractive optical element. The revolutionary idea was placing the combining element inside the resonant cavity, avoiding wavelength changes caused by cavity instabilities.

13. Taji resonator: towards integrated unidirectional reflector (Fabio Turri, Fernando Ramiro Manzano)

An interesting topic than can be deepened with integrated Silicon devices is optical insulation and the possibility to create integrated devices showing asymmetric losses. In this view, a peculiar type of resonator has been ideated, fabricated and characterized to demonstrate its unidirectional/asymmetric response.
A sketch of the resonator can be seen in Fig. 16 (left), where three fundamental parts can be recognized: (1) a bus waveguide used to connect the device with the external circuit, (2) a common optical ring resonator coupled to the waveguide, and (3) a central S-shaped waveguide coupled to the resonator. The shape recalls that of the Taji symbol, the name of the device thus coming from this similarity. From the theoretical model and the simulations, its output is expected to vary depending on the input direction. In particular, while the symmetry of the system is not broken for the transmitted signal, reflectance output should depend on the input direction. In Fig. 16 (center-right) the resonator output is shown for mode excitation from the left port (central figure) or from the right port (right figure) of the bus waveguide: while similar transmittance signals are observed (red curve), very different reflectance signals are found (green curve) making the device a unidirectional reflector (in the simulation low propagation losses has been considered with respect to losses coming from the S-shaped waveguide). This comes from the different dissipation channels of the ring: the additional S-branch becomes a source of losses only when light propagates in the clockwise mode (i.e. when the light enters the S-branch), thus creating the asymmetry.

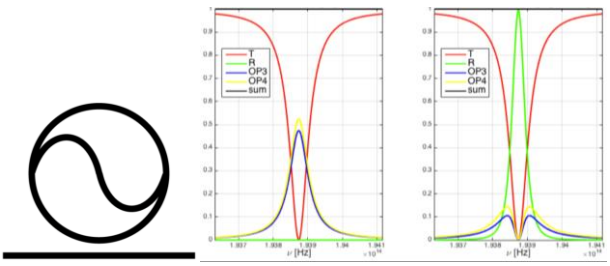

Figure 16. *Sketch of the Taji resonator (left) and predicted resonator output from the theoretical model in the case of a critically coupled resonator excited from the left(center)/right(right) port of the bus waveguide.*

Experimental validation of the model has been performed with SiON based resonators, where the fabrication/coupling parameters have been chosen to maximize the unidirectionality of the system. In Fig. 17 a sketch of the actual device is shown, where reflection killers at the end of the S-branch and directional couplers as coupling elements have been introduced to achieve better performance of the S-branch element. In Fig. 17 (bottom panel), the experimental results are shown. Excitation of the ring mode has been provided from two directions and both the reflectance and the transmittance have been acquired simultaneously. Spectra in the top

panel belongs to the "working Taji" configuration, when the S-branch is crossed by a large fraction of the light signal travelling in the resonator. From a comparison of the two panels, the asymmetric response of the device becomes evident: the reflected signal (red curves) shows well marked peaks in correspondence of the transmittance peaks only when the S-branch works, as in the model prediction (i.e. when the left port is used to excite the system). Conversely, the transmitted signal does not show significant variations between the two configurations, recalling the typical resonance peaks associated to an all-pass filter (different amplitudes and shapes due to different alignment of the injection fibers/facets).

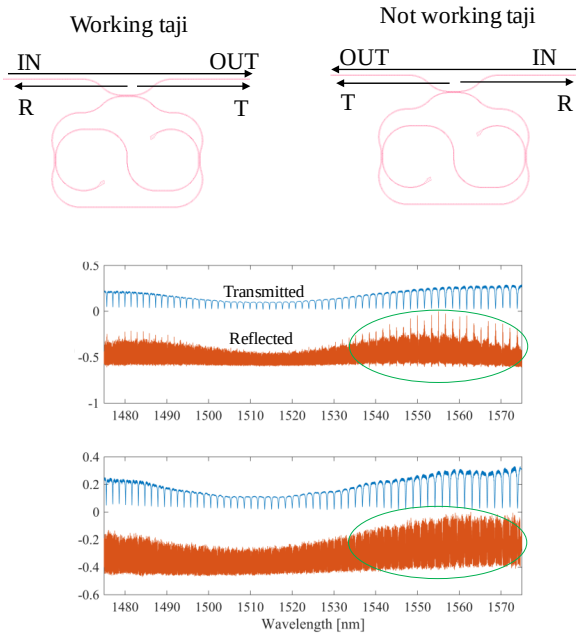

Figure 17. *Transmitted (blue) and reflected (red) signals for the "working Taji" (top) and "not-working Taji" (bottom) configurations; the green circles highlight the spectral region where the difference between one and the other configurations is more marked (losses in other spectral region becomes predominant and hides the Taji behavior).*

14. Second-harmonic generation in stressed microring resonators (Chiara Vecchi, Pierre Guillemé)

Optical frequency combs (OFCs) are light sources whose spectrum contains thousands of equally spaced laser lines. They have revolutionized precise optical frequency measurements by making possible to directly link any optical frequency to a microwave clock. Nowadays, they are the indispensable equipment for many other applications, ranging from synchronization of telecommunication systems to astronomical spectral calibration and biomedical or environmental spectrometry. It should also be noted that the self-referencing allowed by octave spanning OFCs was awarded with the Physics Nobel Prize in 2015.

Recent experiments have demonstrated that OFCs may arise entirely through second-order nonlinear optical effects which potentially requires low pump power and intrinsically leads to an octave span. In this scheme, the pump signal generates a Second Harmonic (SH) which undergoes an optical parametric oscillation giving birth to new frequencies around the pump one. If the dispersion is correctly engineered, when the pump power becomes large enough, the process repeats itself to generate an OFC.

In the NEMO national project, we propose to exploit the technological versatility of Silicon to develop on-Silicon chip-based OFC sources relying on second-order optical nonlinearity. Specifically, we study here microring resonators of Silicon-on-Silica substrate. Nevertheless, the centrosymmetry of this material needs to be artificially broken to prevent its second-order nonlinear susceptibility $\chi^{(2)}$ to vanish. To this aim, a silicon nitride layer induces an inhomogeneous strain to the Silicon lattice preventing the $\chi^{(2)}_{zxy}$ term of the susceptibility tensor to vanish.

To achieve SHG, three conditions must be fulfilled. First the energy conservation imposes that the SH wavelength is half the fundamental one. Then, since we assume that the SHG is allowed by the $\chi^{(2)}_{zxy}$ term, the fundamental electric field must be in the microring plane (TE polarized) and the SH electric field will be generated along the axis of the ring (TM polarized). Finally, the phase matching condition imposes that the azimuthal numbers respect $m_{SH} = 2m_f + 2$. Besides, to take opportunity of the modal phase matching, we considered modes with a radial number $p = 3$ for the SH. Finally, to prevent two photon absorption the fundamental wavelengths are chosen above 2.2 µm.

The resonant modes exhibiting the correct polarizations and azimuthal number relation are determined by FEM simulation and an optimization program varies the ring radius till the energy conservation is achieved. The points on Fig. 18 shows some of the conditions allowing SHG obtained this way. We see that a large choice of geometries is available for radii above 10 µm, widths around 900 nm and thicknesses ranging from 270 nm to 300 nm. Moreover, this first study shows that increasing the thickness *e* or the width *w* of the system requires to use larger fundamental wavelengths. If these two geometrical parameters are fixed, increasing the radius also requires to increase the pump wavelength.

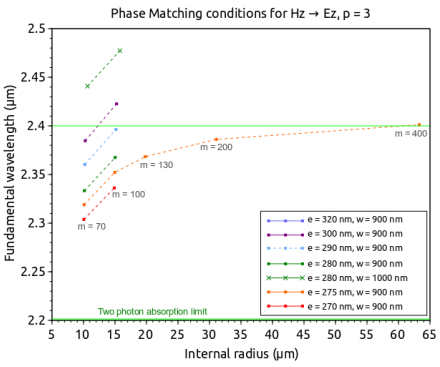

Figure 48. *Conditions allowing SHG in the case where a fundamental TE mode generates a TM mode with a radial number 3. e and w are the thickness and the width respectively.*

Among the numerous sets of parameters allowing SHG, the ones selected for the experimental realization should meet three requirements: exhibiting the best conversion efficien-

cies, a slight anomalous dispersion and sizes for the coupling with external bus compatible with our technical limits. The next three paragraphs will detail these points.
The estimation of the conversion efficiency takes into account, on one hand, the overlap between the fundamental and the SH modes and, on the other hand, the ratio of power coupled between the external bus and the microresonator. The overlap is calculated from the FEM simulation of the modes while the coupling ratio is given assuming both intrinsic and coupling quality factors to be 10^4. For 1 mW pump power and taking $\chi^{(2)}_{zxy}$ = 1 pm/V, the conversion efficiency η is shown on Fig. 19. It is around half 1 %.mW^{-1}. It increases with the thickness but decreases with the width or the radius.

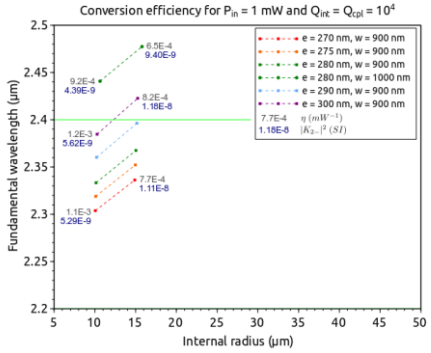

Figure 19. *Conversion efficiencies for 1 mW pump power and Q-factors 10^4 in different conditions allowing SHG.*

When an error on the radius is made during the fabrication process, the conditions for SHG are not fulfilled and η drops of several orders of magnitude as shown on Fig. 20. The blue curve is obtained by keeping the pump wavelength fixed at the value calculated for the correct size of the microring, while the red (green) one is obtained by tuning the wavelength to keep the pump resonant with the same azimuthal number (the following azimuthal number). An error of 5 nm divides η by 50 and an error of 10 nm by 200.

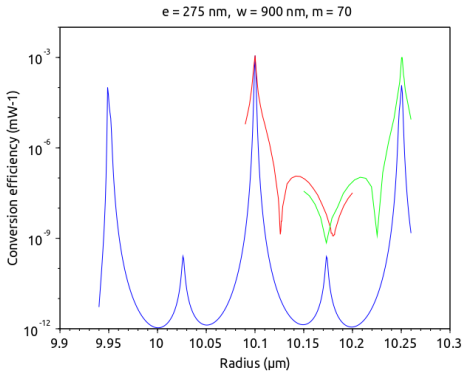

Figure 20. *Conversion efficiency for radii which do not respect the conditions for SHG.*

The successive SHG, OPO and sum frequency generations can lead to an OFC if the free spectral range remains constant over one octave. This is possible only if the dispersion is slightly anomalous. Fig. 21 shows that the dispersion can be engineered by modifying the aspect ratio: when *w/e* gets closer to 1 (squared cross section) the dispersion increases. The orange case [*e* = 275 nm, *w* = 900 nm] has been selected for the first experimental realization.

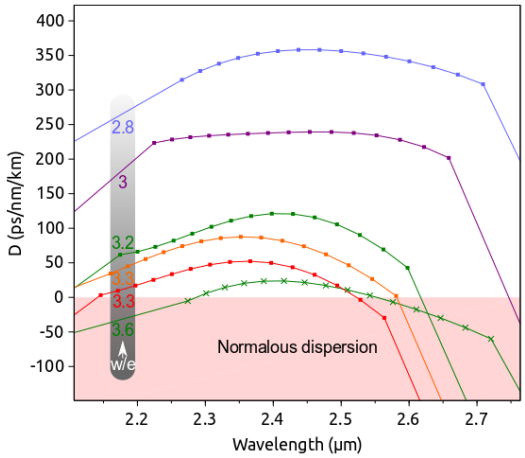

Figure 21. *Dispersion parameter of microresonators exhibiting different geometries corresponding to the legend of figure 1.*

For this case, the possible pulley coupling has been investigated by checking that for a gap of 500 nm, the coupling length required to achieve critical coupling for both fundamental and SH is reasonable. First, we determined the width of the waveguides allowing phase matching between the mode propagating in the microresonator and the one propagating in the bus. Then the FEM simulation allowed the computation of the coupling coefficient between these modes. Finally, we determined the length needed to couple the amount of power that compensates the one lost in the microring for an intrinsic Q-factor of 10^4. The coupling length is around 1 µm for the fundamental and 7 µm for the SH which corresponds to a small portion of the microring circumference. The optical characterization of this first set of microresonators will allow to consider more realistic parameters for the next simulations of the OFC in order to correctly design the final samples.

15. Investigating the origin of second order nonlinearities in strained silicon waveguides (Claudio Castellan, Alessandro Trenti, Chiara Vecchi, Alessandro Marchesini, Mattia Mancinelli)

Centrosymmetry inhibits second order nonlinearities in centrosymmetric crystals, like silicon. However, the application of a stressing layer on top of a silicon waveguide has shown the capability to introduce second order nonlinearities. We have investigated the Second Harmonic Generation (SHG) process in a strained silicon waveguide engineered to achieve the multimodal phase-matching. In this way, we determined a second order nonlinear coefficient of about 0.3 pm/V. Nevertheless, the origin this nonlinearity is still under debate. In fact, it can be due not only to a breaking of the silicon centrosymmetry caused by strain, but it can also have other origins, related for example to the field induced by trapped charges or to the generation in the silicon nitride cladding.
In order to remove these doubts, we are going to repeat the SHG experiments described so far using a sample holder equipped by a screw, as it is shown in Fig. 22a. In this way, a tunable mechanical strain is introduced in the waveguide. Studying the generation efficiency as a function of the applied load will provide a clear proof of the role that strain

has on second order nonlinearities. Moreover, we will find a relationship between the strain-induced nonlinearity and the nonlinearity induced by other phenomena. Using a FEM software, we can determine the strain into the waveguide. As an example, in Fig. 22b we report the strain distribution inside a waveguide stressed by the screw, which is applying a displacement of 0.15 mm in the center of the sample. The comparison of the simulations and the experiment will provide the relationship between strain and the strain-induced second order nonlinearity.

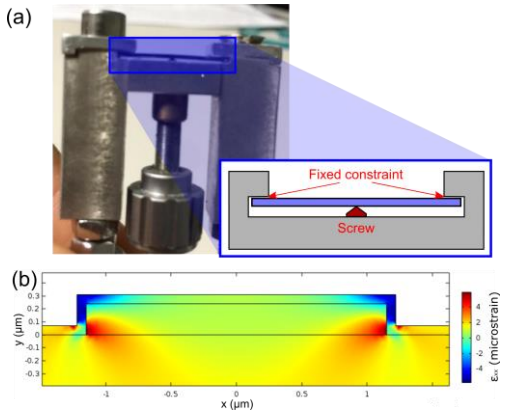

Figure 22. *(a) Sample holder equipped by the screw. (b) The strain distribution inside a waveguide stressed by the screw*

16. Tunable resonance shift in silicon racetrack resonators applying variable strain (Claudio Castellan, Astghik Chalyan)

The role played by strain on the performance of integrated devices is of extreme interest. One of the reasons for this comes from the development of flexible devices. Especially in the field of flexible electronics, many material platforms have been demonstrated, providing high device performance even when subjected to stretching or compression. In this work [1], we analyze the role of strain on silicon racetrack resonators, where loading is applied in a controlled way by using a micrometric screw (Fig.22) to cause the sample to bend.

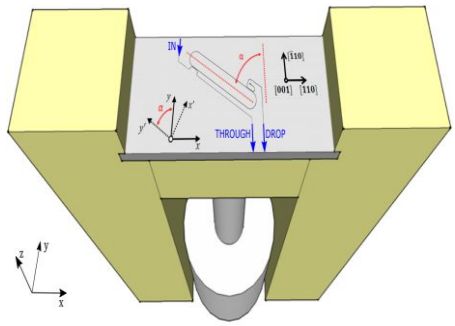

Figure 22. *Zoom-in picture of the screw-equipped sample holder. On the sample it is depicted a resonator whose main axis is rotated of an angle α with respect to the y direction. The resonator dimensions are deliberately out of scale.*

We discuss the role played by the resonator orientation with respect to the applied strain, showing that the strain-induced resonance wavelength shift can be tuned from positive to negative values by changing the orientation angle. This offers interesting applications in the field of strain sensors, since different orientations of the resonators on the same sample can provide information on the strain direction. Moreover, choosing the orientation angle to manufacture a strain-insensitive resonator is of extreme interest in the field of flexible photonics, where it is necessary to produce devices insensitive to the applied strain. In this framework, we describe the experimental results, taking into account the different effects responsible for the resonance shift. Our model considers both mechanical deformation of the device, which affects the resonator perimeter and the waveguide cross-section, and the strain-induced refractive index variation, due to the photoelastic effect. We performed Finite element simulations taking into account all these effects are presented, providing good agreement with experimental results. By studying the role of the resonator orientation we identify interesting features, such as the tuning of the resonance shift from negative to positive values and the possibility of realizing strain insensitive devices.

References

1. Claudio Castellan, Astghik Chalyan, Mattia Mancinelli, Pierre Guilleme, Massimo Borghi, Federico Bosia, Nicola M. Pugno, Martino Bernard, Mher Ghulinyan, Georg Pucker, and Lorenzo Pavesi, "Tuning the strain-induced resonance shift in silicon racetrack resonators by their orientation," Opt. Express 26, 4204-4218 (2018)

For more info

Nanoscience Laboratory
Department of Physics
University of Trento
via Sommarive 14
38123 Povo- Trento (Italy)
http://nanolab.physics.unitn.it/

secretary dr. Tatsiana Egorova
email tatsiana.egorova@unitn.it
phone +390 461 283172